Tunable Infrared Phonon Anomalies in Trilayer Graphene

Chun Hung Lui (呂振鴻),[1] Emmanuele Cappelluti,[2,3] Zhiqiang Li,[1] and Tony F. Heinz[1]

[1]*Departments of Physics and Electrical Engineering, Columbia University, 538 West 120th Street, New York, New York 10027, USA*
[2]*Istituto dei Sistemi Complessi (ISC), CNR, U.O.S. Sapienza, v. dei Taurini 19, 00185 Rome, Italy*
[3]*Instituto de Ciencia de Materiales de Madrid (ICMM), CSIC, Cantoblanco, 28049 Madrid, Spain*

(Received 21 January 2013; published 1 May 2013)

Trilayer graphene in both *ABA* (Bernal) and *ABC* (rhombohedral) stacking sequences is shown to exhibit intense infrared absorption from in-plane optical phonons. The phonon feature, lying at $\sim$1580 cm^{-1}, changes strongly with electrostatic gating. For *ABC*-stacked graphene trilayers, we observed a large enhancement in phonon absorption amplitude, as well as softening of the phonon mode, as the Fermi level is tuned away from charge neutrality. A similar, but substantially weaker, effect is seen in samples with the more common *ABA* stacking order. The strong infrared response of the optical phonons and the pronounced variation with electrostatic gating and stacking order reflect the interactions of the phonons and electronic excitations in the two systems. The key experimental findings can be reproduced within a simplified charged-phonon model that considers the influence of charging through Pauli blocking of the electronic transitions.

DOI: 10.1103/PhysRevLett.110.185504 PACS numbers: 63.22.Rc, 63.20.kd, 73.22.Pr, 78.67.Wj

Trilayer graphene has attracted much recent attention because of its unusual electronic properties. This interest is further heightened by the existence of two stable allotropes, the *ABA* and *ABC* stacked trilayers (Fig. 1) [1–4], which exhibit very different characteristics from one another, as well as from monolayer and bilayer graphene. Indeed, the two trilayer allotropes have been shown to possess distinctive electronic and transport properties [1–29]. With respect to phonons, one would, however, expect the in-plane phonons in trilayer graphene to exhibit little sensitivity to stacking order (or changed layer thickness) because of the weak interlayer lattice coupling [30].

In contrast to such an expectation of weak structure dependence for phonons, we show here that the infrared (IR) spectra of in-plane optical phonons in trilayer graphene are dramatically modified both by stacking order and charge density. We observe noticeable IR absorption by the zone-center in-plane optical phonons in both trilayer allotropes around 1580 cm^{-1}, but with distinct characteristics and variation with electrostatic gating. As we tune the Fermi level to either the electron or hole side, we record a strong enhancement in the IR absorption amplitude accompanied by a significant softening ($\sim$15 cm^{-1}) of the phonon mode in *ABC* trilayers. In contrast, the *ABA* trilayers show much weaker phonon features and a less pronounced response to doping. We are able to reproduce the key experimental observations within a model based on charged-phonon theory. Our analysis shows that the observed IR response of the optical phonons arises from their interactions with the interband electronic transitions. The increased response and greater sensitivity to doping in the *ABC* graphene trilayers reflects the presence of stronger low-energy electronic transitions compared with the *ABA* system. The measurements complement previous studies of few-layer graphene samples at fixed doping [31] and also studies of bilayer graphene, which exists in only one allotrope, at variable doping [32,33]. Our exploration of the IR phonon anomaly with respect to both the stacking and doping degrees of freedom reveals the significant interplay between the two variables in the system, which is not anticipated by the previous studies. The strikingly different doping dependence for *ABA* and *ABC* trilayers reflects the distinct electron-phonon interactions in these two allotropes. More generally, the phenomenon of structural dependence of doping-induced IR phonon anomalies, as demonstrated in our experiment, should prevail in graphene systems of greater thickness because of the range of stacking orders in these materials.

In our experiment, graphene trilayer samples were prepared by mechanical exfoliation of kish graphite (Covalent Materials Corp.) on SiO_2(300 nm)/Si substrates. The sample thickness and the stacking order were characterized by means of IR and Raman spectroscopy [1–4,11]. All IR measurements in our experiment were performed using the National Synchrotron Light Source at Brookhaven National Laboratory (U12IR beam line). We further used the signature of the stacking order in the 2D Raman feature to map out the stacking domains of the trilayer samples by Raman imaging [2]. We chose those samples with large (> 200 μm^2) homogeneous domains of *ABA* or *ABC* stacking for device fabrication. We made use of polymer electrolyte (poly(ethylene oxide):$LiClO_4$) top gates, which allowed us to induce high doping densities ($\sim 10^{13}$ cm^{-2}) in the trilayer graphene samples. Details of the device fabrication are provided in Refs. [3,34].

We measured the IR transmission spectrum of the gated trilayers at near-normal incidence by comparing spectra taken from regions of the substrate with and without the

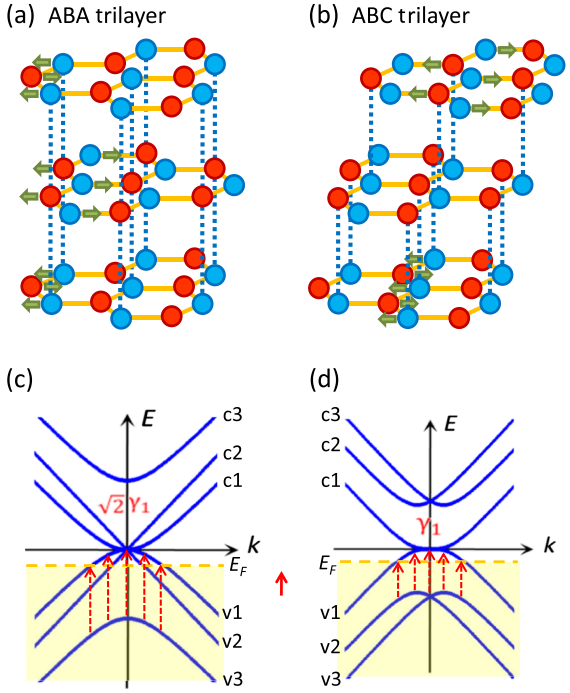

FIG. 1 (color online). (a)–(b) Lattice structure of trilayer graphene with *ABA* (a) and *ABC* (b) stacking order. The red and blue dots represent carbon atoms in the *A* and *B* sublattices of the graphene honeycomb structure. The arrows represent the atomic displacements of the major IR active optical phonon modes: E'_b mode in *ABA* trilayer and E_u mode in *ABC* trilayer. (c)–(d) Band structure of graphene trilayers with *ABA* (c) and *ABC* (d) structure based on a tight-binding model with only γ_0 and γ_1 intra- and interlayer couplings. The conduction and valence bands are symmetric and the energy separations between the low-lying bands and the high-lying bands are approximately $\sqrt{2}\gamma_1$ and γ_1 for *ABA* and *ABC* trilayer, respectively. The dashed red arrows show the most important virtual transitions that contribute to the renormalization of the IR active phonons at finite doping. The solid red arrow between panels (c) and (d) indicates the energy of the zone-center optical phonon.

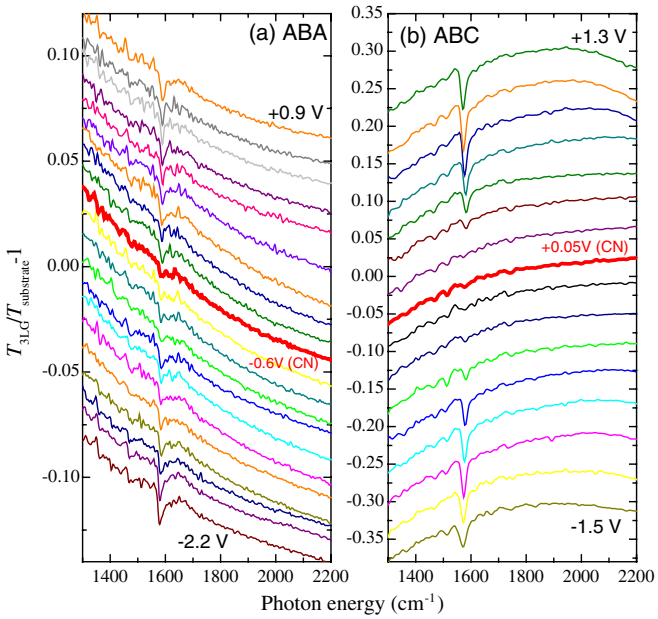

FIG. 2 (color online). (a)–(b) Infrared transmission spectra, displaced for clarity, of trilayer graphene with *ABA* (a) and *ABC* (b) stacking order for different gate voltages V_g. The spectra at the charge neutrality (CN) points, at gate voltage V_{CN}, are highlighted. From top to bottom, the gate voltages for the *ABA* spectra are $V_g = 0.9$, 0.7, 0.5, 0.3, 0.1, −0.1, −0.3, −0.4, −0.5, −0.6 (CN), −0.7, −0.8, −0.9, −1.0, −1.1, −1.2, −1.4, −1.6, −1.8, −2.0, and −2.2 V; The gate voltages for the *ABC* spectra are from top to bottom: $V_g = 1.3$, 1.2, 1.0, 0.8, 0.6, 0.4, 0.2 0.05 (CN), −0.1, −0.3, −0.5, −0.7, −0.9, −1.1, −1.3, and −1.5 V.

trilayer graphene sample. Figures 2(a) and 2(b) display the fractional change in transmission for *ABA* and *ABC* trilayers for different gate voltages (V_g). In the transmission spectra of both trilayers, we identify a sharp feature at ∼1580 cm^{-1}, the energy of the zone-center optical phonons. The slope in the spectra arises from the trilayer electronic response, as well as from residual absorption of the polymer top gate for which lateral thickness variation makes the normalization to the substrate imperfect. The electronic contribution, arising from absorption by the direct electronic transitions in the graphene trilayer, has been discussed in detail in Refs. [2,3,35,36]. In order to focus on the phonon feature, we subtracted a smooth baseline using a polynomial fitting procedure.

In our experimental geometry, i.e., a thin film of graphene on a SiO_2(300-nm)/Si substrate, the IR transmission is related to both the real and imaginary parts of the optical conductivity of trilayer graphene. We have applied a Kramers-Kronig constrained variational spectral analysis with the RefFit software developed by Kuzmenko [33,37] to extract the real part of the optical conductivity $\Delta\sigma(\hbar\omega)$ of the trilayer samples, taking into account the known optical constants and thicknesses of the SiO_2 and Si layers. In the calculation, we neglect for simplicity the effect of the thin polymer top-gate layer in our devices. This approximation introduces a few percent error in the absolute magnitude of the inferred IR absorption, but has a negligible effect on the linewidth and line shape of the sharp phonon feature [36].

Figures 3(a) and 3(b) display the differential sheet conductivity spectra $\Delta\sigma(\hbar\omega)$ in the range of 1430–1730 cm^{-1} extracted from the corresponding baseline-corrected transmission spectra in Figs. 2(a) and 2(b). A striking feature of our results is the strong gate induced enhancement of the phonon absorption peak for the *ABC* trilayer graphene [Fig. 3(b)]. The *ABC* trilayer does not show any noticeable absorption peak at the charge neutrality (CN) point, $V_g = V_{CN}$. As V_g is tuned away from V_{CN}, however, a clear absorption feature appears at the zone-center optical phonon energy (∼1580 cm^{-1}) and grows dramatically with the gate bias. For the highest doping levels, the strength of the phonon absorption is comparable to that of the main electronic transition peak at 370 meV [36].

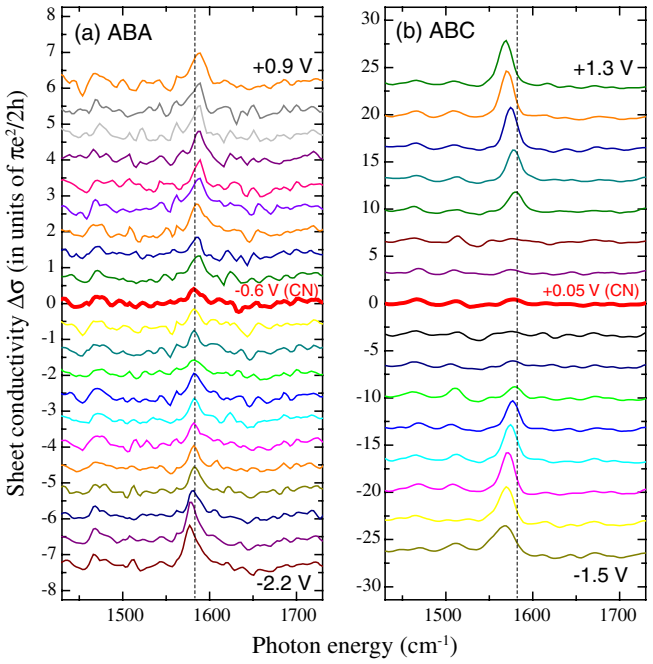

FIG. 3 (color online). (a)–(b) The optical sheet conductivity spectra $\Delta\sigma(\hbar\omega)$ extracted from the corresponding baseline-adjusted transmission spectra in Figs. 2(a) and 2(b). The dashed lines are guides to the eye to show the shift of the phonon energy.

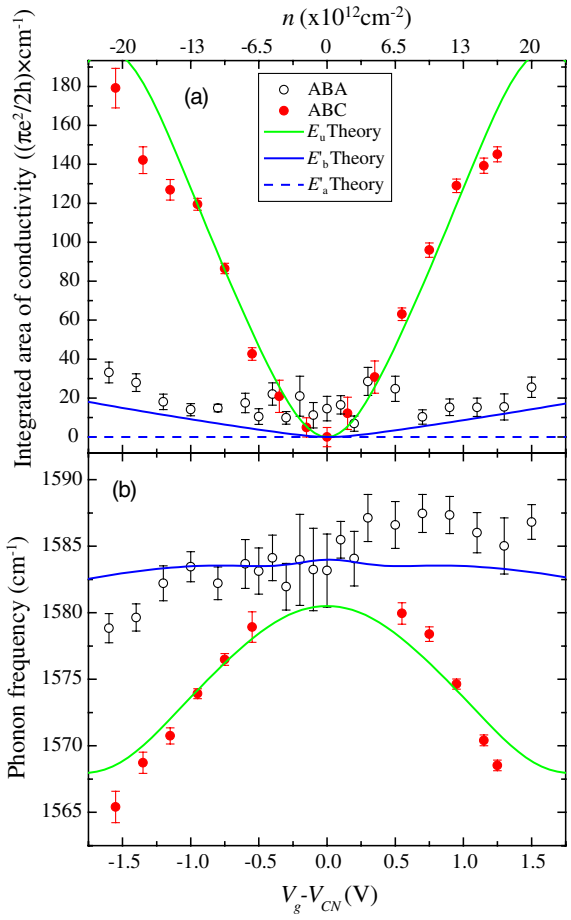

FIG. 4 (color online). The integrated optical sheet conductivity (a) and the phonon frequency (b) extracted from the spectra in Figs. 3(a) and 3(b) by using a single-Lorentzian fitting, displayed as a function of gate voltage (V_g, bottom axis) and of the doping charge density (n, top axis). The symbols are experimental data and the lines are from the charged-phonon model described in the text. The error bars represent the uncertainty in fitting the spectra. The values of V_{CN} are subtracted from V_g for better comparison of the *ABA* and *ABC* data. In (a), we show the calculated spectral intensities of both the E'_a and E'_b modes in the *ABA* trilayer. We see that the E'_b mode has much higher IR activity than the E'_a mode. For the theoretical fits in (b), we assume zero-doping phonon frequencies of 1584 and 1580.5 cm^{-1} for *ABA* and *ABC* trilayers, respectively.

In addition, we observe a red shift of the absorption peak by more than 10 cm^{-1} for both electron and hole doping. We also observe the presence of a phonon absorption peak in *ABA* graphene trilayers [Fig. 3(a)]. The amplitude and frequency of the phonon feature in *ABA* trilayer, however, varies relatively weakly with V_g. Although both *ABA* and *ABC* trilayers have similar absorption strength at low doping, the *ABC* phonon absorption is more than five times greater than the *ABA* absorption at high doping. We have fit each $\Delta\sigma(\hbar\omega)$ spectrum in Figs. 3(a) and 3(b) with a single Lorentzian function and extracted the phonon spectral weight and frequency as the integrated area and peak position of the fit function, respectively. (In contrast to measurements of the optical phonons in bilayer and other few-layer graphene systems [31–33], only slight asymmetry was observed in the spectral line shapes and we do not need to introduce a Fano line shape to describe the results.) The contrast in behavior of the two types of trilayers can be seen clearly in Figs. 4(a) and 4(b), which display the fit parameters as a function of gate voltage. We note that we did not observe any systematic dependence of the spectral linewidth on the gate bias for both types of trilayers.

The observation of strong phonon absorption in graphene trilayers, one that is of similar strength to the direct electronic transitions [36], is striking. Since graphene trilayers are non-polar materials, the electrons are evenly distributed among all the carbon atoms and do not exhibit any significant static dipole moment. Upon doping the additional charges are somewhat unequally distributed on the atomic sites. We estimate, however, that the resulting dipole moments are still 2 orders of magnitude smaller than what is needed to explain the observed strength of phonon absorption. For a proper explanation of the phenomenon, we must consider the interactions between the phonons and electrons in the system. These interactions also allow us to understand the correlation between enhancement of the electronic absorption and the phonon absorption, as well as the large redshift of the phonon absorption peak, with doping. When the IR active phonons are coupled to the electronic transitions, their frequency will be modified and some of the oscillator strength of the electronic transitions can be transferred to the phonon system. The phonons can be considered to be dressed by the electrons, which bestow

additional oscillator strength on them. This so-called charged-phonon absorption [38–40] has also been observed in other systems, including bilayer and few-layer graphene [31–33], C_{60} compounds [41], graphite [42], and some organic materials [43].

For quantitative analysis of our experimental data, we applied charged-phonon theory [38–40] to calculate the spectral properties of the IR active phonons in the *ABA* and *ABC* trilayer systems [36]. This theory, applied successfully in bilayer graphene [39,40], allows us to obtain the absorption strength and the frequency shift induced by the electron-phonon interaction for each phonon mode in trilayer graphene from the real parts of the current-phonon response function and the phonon self-energy, respectively. To capture the key features of the phonon spectra, we adopt a simple model of the electronic structure based on a tight-binding scheme of the electronic structure that includes only the dominant intralayer (γ_0) and interlayer (γ_1) coupling [Figs. 1(c) and 1(d)]. We assume that the only effect of the gating is to modify the electron (hole) population within a rigid-band scheme, neglecting the influence of any gate-induced electric field across the graphene layers. We shall see, despite the simplicity of this model, it is able to account for all the main spectral features in our experiment.

In the absence of perpendicular electric fields, we can identify two IR active phonon modes E'_a and E'_b for the *ABA* trilayer and a single IR active phonon mode E'_u for the *ABC* trilayer [44]. Figures 1(a) and 1(b) display the atomic displacements of E'_b mode for *ABA* structure and E'_u mode for *ABC* structure. In our analysis, we compare the properties of these two modes. The E'_a mode in *ABA* trilayer, which has the same atomic displacement with E'_b except that the atoms in the middle layer move in opposite direction, has much lower IR activity than E'_b mode and can be disregarded in our analysis [Fig. 4(a)].

The calculated phonon spectral weight and frequency of the E'_b mode in *ABA* structure and of E_u mode in *ABC* structure are shown in Figs. 4(a) and 4(b). To fit the experimental data as a function of gate voltage, we used for both devices a top-gate capacitance of $C = 2.6\ \mu\mathrm{F\,cm^{-2}}$. This yielded, for the highest gate voltages in our measurements, an induced charge density of $n = 2.0 \times 10^{13}\ \mathrm{cm^{-2}}$, corresponding to a Fermi energy of $E_F = 290$ meV for the *ABC* trilayer. As shown in Fig. 4(a), our calculation reproduces well the phonon absorption amplitude for the two types of trilayers, with strong gate dependence in the *ABC* system and a weaker dependence in the *ABA* system. A similar behavior is also observed for the frequency shift of the two modes, as evaluated by the phonon self-energy [Fig. 4(b)]. This similarity reflects the fact that both dependences are related to virtual interband particle-hole excitations [39,40]. According to our calculation, the redshift of the phonon frequency arises from coupling of the phonons to electronic transitions of higher energies, the phase space of which increases with doping.

There are numerous possible interband electronic transitions in the trilayers. However, because of the symmetry of the IR active phonons, only a few of them make significant contributions to the IR phonon response. In particular, optical transitions between the low-lying states, such as the v1-c1 transition in Figs. 1(c) and 1(d), are forbidden by selection rules. Also, the pairs of interband transitions that are symmetric under electron-hole exchange, such as the v1-v2 and c1-c2, v1-c2 and v2-c1, as well as v1-c3 and v3-c1 transitions, tend to cancel each other in their influence to the IR phonons [39,40]. As we have adopted a band structure that is symmetric on the electron and hole sides, our theory predicts zero IR activity for the phonons at zero doping and arbitrary temperature. Effective electron-hole transitions will, however, be induced by doping that increases the space of Pauli-allowed transitions and diminishes the destructive interference between different transitions. Our calculation shows that the main contribution to the phonon absorption comes from the electronic transitions between the low- and high-lying conduction (valence) bands, as indicated by the arrows in Figs. 1(c) and 1(d). The principal distinction between the *ABA* and *ABC* electronic structure is thus the energy separation between the low- and high-lying bands, which is approximately $\sqrt{2}\gamma_1 \sim 0.52$ and $\gamma_1 \sim 0.37$ eV for *ABA* and *ABC* trilayers, respectively. The effect of the coupling with such particle-hole excitations will consequently be considerably stronger in the *ABC* structure, which is more nearly resonant with the phonon energy (~ 0.2 eV).

It is also interesting to compare our trilayer results with results previously reported for bilayer graphene [22]. For the same doping density of $1 \times 10^{13}\ \mathrm{cm^{-2}}$, the integrated sheet conductivity of the IR phonon feature normalized by the layer number, is ~ 11 in units of $(\pi e^2/2h) \times \mathrm{cm^{-1}}$ for bilayer graphene [22]. This value is larger than the corresponding one in *ABA* trilayer (~ 5.5), but smaller than that in *ABC* trilayer (~ 33). These differences reflect the more nearly resonant coupling of the optical phonon and interband transitions in the bilayer than in the *ABA* trilayer, but the still stronger interaction of optical phonons with electronic transitions in the *ABC* trilayer.

In our experiment, we observe a weak IR absorption in the *ABA* trilayer at V_{CN} that is not expected by our theory. Such residual absorption may reflect the inhomogeneous spatial distribution of charges expected in real experimental samples and the asymmetry in the band structure of the *ABA* trilayer [3,9] that allows particle-hole excitations to be coupled to the phonons in the absence of doping. Further study of the subject also requires the consideration of the gate induced perpendicular electric field, which is expected to lower the symmetry of the crystals and hence induce IR activity of all three in-plane optical modes even at the charge neutrality point.

In conclusion, our experiment demonstrates that IR response of optical phonons in *ABC* trilayers is much more sensitive to doping than in *ABA* trilayers. The observation reflects the different nature of the coupling of the

phonons with electronic transitions in the two types of trilayer graphene. The results can be explained by a simple theory that considers only the dominant IR active phonon modes and the influence of band filling effects. Previous studies [32,33] have also shown an enhanced phonon absorption and energy redshift with doping in bilayer graphene. Our present results show thus that in this regard the *ABC* trilayer is rather similar to bilayer graphene, but that the *ABA* trilayer stands as a new system in its own right. Such contrast in behavior as a function of stacking order parallels that found in studies of gate-induced band gap opening in bilayer and trilayer graphene [3,34,45,46].

We acknowledge G. L. Carr and R. Smith for technical assistance in the infrared measurements, and A. B. Kuzmenko for important support in the Kramers-Kronig constrained variational analysis of the optical spectra. E. C. acknowledges the Marie Curie Grant No. PIEF-GA-2009-251904. This work was supported by the National Science Foundation (Grant No. DMR-1106225) and by the graphene MURI program of the Office of Naval Research.

[1] K. F. Mak, J. Shan, and T. F. Heinz, Phys. Rev. Lett. **104**, 176404 (2010).
[2] C. H. Lui, Z. Li, Z. Chen, P. V. Klimov, L. E. Brus, and T. F. Heinz, Nano Lett. **11**, 164 (2011).
[3] C. H. Lui, Z. Li, K. F. Mak, E. Cappelluti, and T. F. Heinz, Nat. Phys. **7**, 944 (2011).
[4] C. X. Cong, T. Yu, K. Sato, J. Shang, R. Saito, G. F. Dresselhaus, and M. S. Dresselhaus, ACS Nano **5**, 8760 (2011).
[5] S. Latil and L. Henrard, Phys. Rev. Lett. **97**, 036803 (2006).
[6] F. Guinea, A. H. C. Neto, and N. M. R. Peres, Phys. Rev. B **73**, 245426 (2006).
[7] M. Aoki and H. Amawashi, Solid State Commun. **142**, 123 (2007).
[8] H. K. Min and A. H. MacDonald, Prog. Theor. Phys. Suppl. **176**, 227 (2008).
[9] M. Koshino and E. McCann, Phys. Rev. B **79**, 125443 (2009).
[10] F. Zhang, B. Sahu, H. Min, and A. H. MacDonald, Phys. Rev. B **82**, 035409 (2010).
[11] C. H. Lui, L. M. Malard, S. Kim, G. Lantz, F. E. Laverge, R. Saito, and T. F. Heinz, Nano Lett. **12**, 5539 (2012).
[12] M. F. Craciun, S. Russo, M. Yamamoto, J. B. Oostinga, A. F. Morpurgo, and S. Tarucha, Nat. Nanotechnol. **4**, 383 (2009).
[13] T. Taychatanapat, K. Watanabe, T. Taniguchi, and P. Jarillo-Herrero, Nat. Phys. **7**, 621 (2011).
[14] A. Kumar, W. Escoffier, J. M. Poumirol, C. Faugeras, D. P. Arovas, M. M. Fogler, F. Guinea, S. Roche, M. Goiran, and B. Raquet, Phys. Rev. Lett. **107**, 126806 (2011).
[15] L. Zhang, Y. Zhang, J. Camacho, M. Khodas, and I. Zaliznyak, Nat. Phys. **7**, 953 (2011).
[16] W. Bao *et al.*, Nat. Phys. **7**, 948 (2011).
[17] S. H. Jhang *et al.*, Phys. Rev. B **84**, 161408 (2011).
[18] S. Yuan, R. Roldán, and M. I. Katsnelson, Phys. Rev. B **84**, 125455 (2011).
[19] E. A. Henriksen, D. Nandi, and J. P. Eisenstein, Phys. Rev. X **2**, 011004 (2012).
[20] M. Koshino and E. McCann, Phys. Rev. B **80**, 165409 (2009).
[21] A. A. Avetisyan, B. Partoens, and F. M. Peeters, Phys. Rev. B **81**, 115432 (2010).
[22] M. Koshino, Phys. Rev. B **81**, 125304 (2010).
[23] F. Zhang, J. Jung, G. A. Fiete, Q. Niu, and A. H. MacDonald, Phys. Rev. Lett. **106**, 156801 (2011).
[24] F. Zhang, D. Tilahun, and A. H. MacDonald, Phys. Rev. B **85**, 165139 (2012).
[25] D.-H. Xu, J. Yuan, Z.-J. Yao, Y. Zhou, J.-H. Gao, and F.-C. Zhang, Phys. Rev. B **86**, 201404 (2012).
[26] R. Côté, M. Rondeau, A.-M. Gagnon, and Y. Barlas, Phys. Rev. B **86**, 125422 (2012).
[27] T. Khodkov, F. Withers, D. C. Hudson, M. F. Craciun, and S. Russo, Appl. Phys. Lett. **100**, 013114 (2012).
[28] R. Ma, L. Sheng, M. Liu, and D. N. Sheng, Phys. Rev. B **86**, 115414 (2012).
[29] M. M. Scherer, S. Uebelacker, D. D. Scherer, and C. Honerkamp, Phys. Rev. B **86**, 155415 (2012).
[30] J. A. Yan, W. Y. Ruan, and M. Y. Chou, Phys. Rev. B **77**, 125401 (2008).
[31] Z. Li, C. H. Lui, E. Cappelluti, L. Benfatto, K. F. Mak, G. L. Carr, J. Shan, and T. F. Heinz, Phys. Rev. Lett. **108**, 156801 (2012).
[32] T. T. Tang *et al.*, Nat. Nanotechnol. **5**, 32 (2009).
[33] A. B. Kuzmenko, L. Benfatto, E. Cappelluti, I. Crassee, D. van der Marel, P. Blake, K. Novoselov, and A. Geim, Phys. Rev. Lett. **103**, 116804 (2009).
[34] K. F. Mak, C. H. Lui, J. Shan, and T. F. Heinz, Phys. Rev. Lett. **102**, 256405 (2009).
[35] N. Ubrig, P. Blake, D. v. d. Marel, and A. B. Kuzmenko, Europhys. Lett. **100**, 58003 (2012).
[36] See Supplemental Material at http://link.aps.org/supplemental/10.1103/PhysRevLett.110.185504 for more information.
[37] A. B. Kuzmenko, Rev. Sci. Instrum. **76**, 083108 (2005).
[38] M. J. Rice, Phys. Rev. Lett. **37**, 36 (1976).
[39] E. Cappelluti, L. Benfatto, and A. B. Kuzmenko, Phys. Rev. B **82**, 041402(R) (2010).
[40] E. Cappelluti, L. Benfatto, M. Manzardo, and A. B. Kuzmenko, Phys. Rev. B **86**, 115439 (2012).
[41] K.-J. Fu, W. Karney, O. Chapman, S.-M. Huang, R. Kaner, F. Diederich, K. Holczer, and R. Whetten, Phys. Rev. B **46**, 1937(R) (1992).
[42] M. Manzardo, E. Cappelluti, E. van Heumen, and A. B. Kuzmenko, Phys. Rev. B **86**, 054302 (2012).
[43] D. B. Tanner, C. S. Jacobsen, A. A. Bright, and A. J. Heeger, Phys. Rev. B **16**, 3283 (1977).
[44] J. A. Yan, W. Y. Ruan, and M. Y. Chou, Phys. Rev. B **79**, 115443 (2009).
[45] Y. B. Zhang, T.-T. Tang, C. Girit, Z. Hao, M. C. Martin, A. Zettl, M. F. Crommie, Y. R. Shen, and F. Wang, Nature (London) **459**, 820 (2009).
[46] A. B. Kuzmenko, I. Crassee, D. van der Marel, P. Blake, and K. S. Novoselov, Phys. Rev. B **80**, 165406 (2009).